

## RESEARCH ARTICLE

# Novel muscle and connective tissue design enables high extensibility and controls engulfment volume in lunge-feeding rorqual whales

Robert E. Shadwick<sup>1,\*</sup>, Jeremy A. Goldbogen<sup>2</sup>, Jean Potvin<sup>3</sup>, Nicholas D. Pyenson<sup>4</sup> and A. Wayne Vogl<sup>5</sup>

<sup>1</sup>Department of Zoology, University of British Columbia, Vancouver, BC, Canada, V6T 1Z4, <sup>2</sup>Cascadia Research Collective, 218 West 4th Avenue, Olympia, WA 98501, USA, <sup>3</sup>Department of Physics, Saint Louis University, 3450 Lindell Boulevard, St Louis, MO 63103, USA, <sup>4</sup>Department of Paleobiology, National Museum of Natural History, Smithsonian Institution, PO Box 37012, MRC 121, Washington, DC 20013-7012, USA and <sup>5</sup>Department of Cellular and Physiological Sciences, University of British Columbia, Vancouver, BC, Canada, V6T 1Z3

\*Author for correspondence (shadwick@zoology.ubc.ca)

### SUMMARY

Muscle serves a wide variety of mechanical functions during animal feeding and locomotion, but the performance of this tissue is limited by how far it can be extended. In rorqual whales, feeding and locomotion are integrated in a dynamic process called lunge feeding, where an enormous volume of prey-laden water is engulfed into a capacious ventral oropharyngeal cavity that is bounded superficially by skeletal muscle and ventral groove blubber (VGB). The great expansion of the cavity wall presents a mechanical challenge for the physiological limits of skeletal muscle, yet its role is considered fundamental in controlling the flux of water into the mouth. Our analyses of the functional properties and mechanical behaviour of VGB muscles revealed a crimped microstructure in an unstrained, non-feeding state that is arranged in parallel with dense and straight elastin fibres. This allows the muscles to accommodate large tissue deformations of the VGB yet still operate within the known strain limits of vertebrate skeletal muscle. VGB transverse strains in routine-feeding rorquals were substantially less than those observed in dead ones, where decomposition gas stretched the VGB to its elastic limit, evidence supporting the idea that eccentric muscle contraction modulates the rate of expansion and ultimate size of the ventral cavity during engulfment.

Key words: ventral groove blubber, collagen, elastin, muscle morphology, Balaenopteridae.

Received 22 October 2012; Accepted 22 March 2013

### INTRODUCTION

Vertebrate skeletal muscle can perform a variety of mechanical roles in locomotor systems. Active shortening contractions provide power for movement by performing ‘positive’ work, whereas muscles that are activated while being lengthened by an external load (eccentric contraction) can develop high forces and absorb energy, as they perform ‘negative’ work (Biewener, 2003; Syme, 2006). These differing and conflicting functions may be performed by anatomically distinct muscles or, alternatively, by the same muscles acting at different times or under different locomotor regimes (Altringham et al., 1993; Gillis and Blob, 2001; Biewener et al., 2004; Higham and Biewener, 2008; Syme, 2006).

Lunge feeding by rorquals (baleen whales of the family Balaenopteridae) is a process that may also involve multiple demands on muscles. This method of bulk filter feeding is one of the most impressive biomechanical events among vertebrates, especially given the extremely large body size of rorquals (Goldbogen et al., 2007; Goldbogen, 2010). In species such as blue (*Balaenoptera musculus*) and fin (*B. physalus*) whales, each lunge takes approximately 6 to 8 s, during which a volume of water as large as or exceeding the entire body volume is engulfed. This amazing feat is achieved by the rapid expansion of a capacious ventral cavity (Fig. 1), bounded by the ventral groove blubber (VGB) superficially and the body wall medially. The VGB is a thick elastic structure composed of several tissue layers, as described by previous investigators (Pivorunas, 1977; Orton and Brodie, 1987). It extends

from the anterior tip of the mandibles near the chin to the umbilicus, a distance that typically spans 50–60% of the entire body length (Goldbogen et al., 2010). The primary constituents of the VGB are blubber (an outer lipid-rich connective tissue layer) and two underlying muscle strata, one with fibre bundles oriented parallel to the body axis [longitudinal stratum (LS)] and another with oblique fibre bundles [oblique stratum (OS)] in multiple layers with alternating angles of ~45 deg to the LS and body axis (Fig. 2). The muscle strata have been described as highly extensible and elastic, due to a high proportion of elastin and collagen (Sokolov, 1960; Orton and Brodie, 1987). Elastin fibres in the blubber are large (1–2 mm diameter) and run at a 45 deg angle to the body long axis (Orton and Brodie, 1987). When expanded, the VGB grooves unfold and can expand by as much as 300% in the circumferential direction (i.e. up to four times the initial dimension). This change is accomplished by stretching of the elastin-rich tissue in the grooves between the relatively inextensible ridges (Orton and Brodie, 1987) (see Fig. 3). The extensible grooves and the ridges are reinforced with stiff collagen fibres that provide the ultimate limit to tissue extensibility, resulting in a steeply non-linear stress–strain curve for this material, and a much lower extensibility in the longitudinal axis.

During steady swimming with a closed mouth, the VGB is held tight against the throat with the grooves closed, such that the thickest part of the body is in the thoracic region rather than below the skull (Williamson, 1972; Arnold et al., 2005). The great expansion of the VGB during engulfment dramatically changes the rorqual body

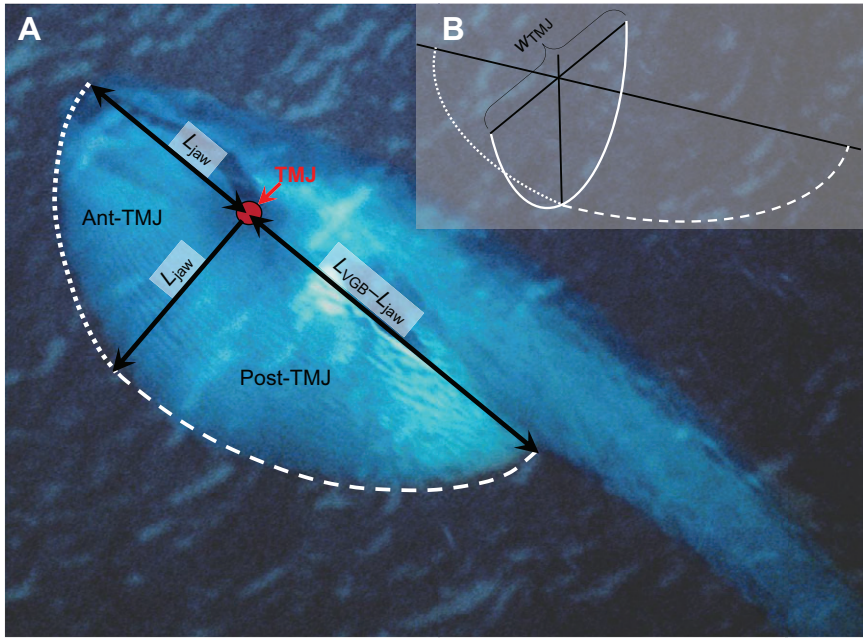


Fig. 1. (A). Image of a blue whale lunge feeding near the surface, showing the ventral cavity fully inflated as it has rolled on its right side. The shape of the cavity is modeled as two quarter ellipsoids; one anterior to the temporomandibular joint (TMJ), and the other posterior to the TMJ. This configuration allows us to estimate the maximal ventral groove blubber (VGB) strain in the longitudinal and transverse directions along the perimeter of the ellipses defined by the axes, as in B. TMJ, the pivot point between the mandible and skull;  $L_{\text{jaw}}$ , the length of the mandible projected in the anterior-posterior body axis;  $L_{\text{VGB}}$ , the total length of the VGB cavity;  $w_{\text{TMJ}}$ , the width between the mandibular condyles when the mouth is open (see also Fig. 4). Photo courtesy of Richard Sears, Mingan Island Cetacean Society.

profile from being highly streamlined to a tadpole-like shape with a consequential 10-fold higher drag (Fig. 1) (Goldbogen et al., 2007; Potvin et al., 2009). The functional properties of the muscle and blubber layers that allow the VGB to undergo this remarkable mechanical transformation are the subject of the present study, specifically the role these muscle layers play during engulfment.

Based on the ease with which the VGB could be stretched in tensile tests, Orton and Brodie (Orton and Brodie, 1987) proposed that if a fin whale's forward speed heading into a lunge was high enough, the dynamic pressure of the water contacting the mouth cavity could be sufficient to completely extend the VGB and inflate the ventral cavity. By approximating the inflated cavity as a thin-

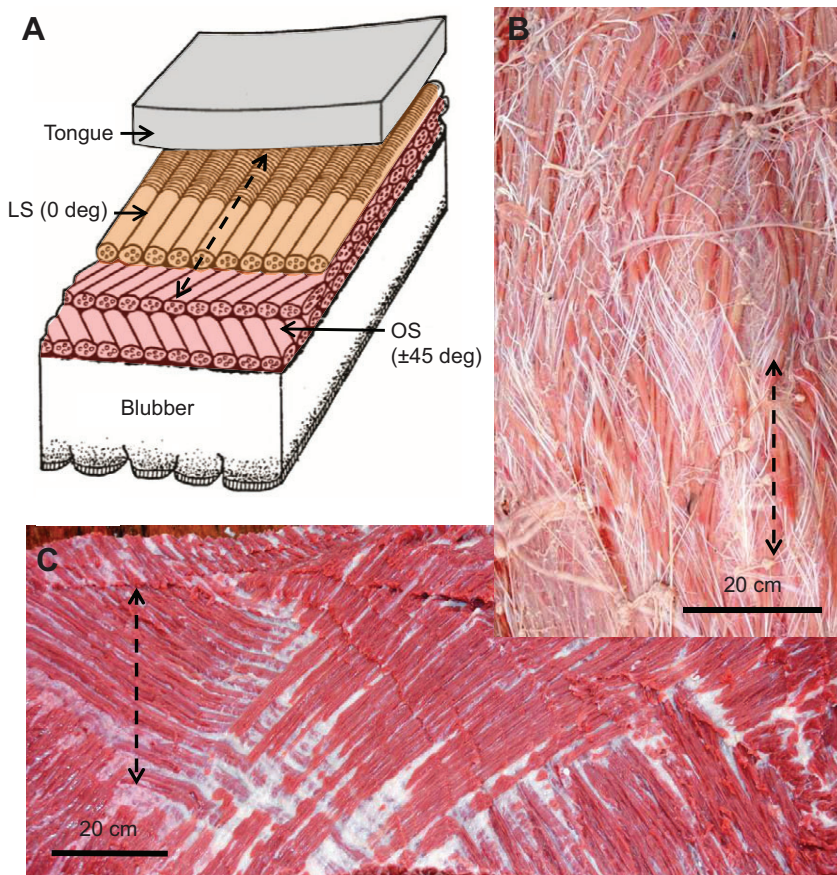


Fig. 2. (A) Two VGB muscle strata are present in the body wall next to the ventral cavity. The oblique stratum (OS) lies under the blubber layer and has alternating layers of fibre bundles oriented at  $\pm 45$  deg to the body long axis, while the longitudinal stratum (LS) lies adjacent and deep to the OS. Reprinted from Orton and Brodie (Orton and Brodie, 1987) with permission. (B) A view of the LS from the deep surface adjacent to the tongue, showing thick muscle bundles (pink) and numerous tendons (white). (C) A view of the OS that has been cut parallel to the blubber layer, showing fibres from two adjacent oblique muscle layers. Dashed arrows indicate the body long axis in each panel.

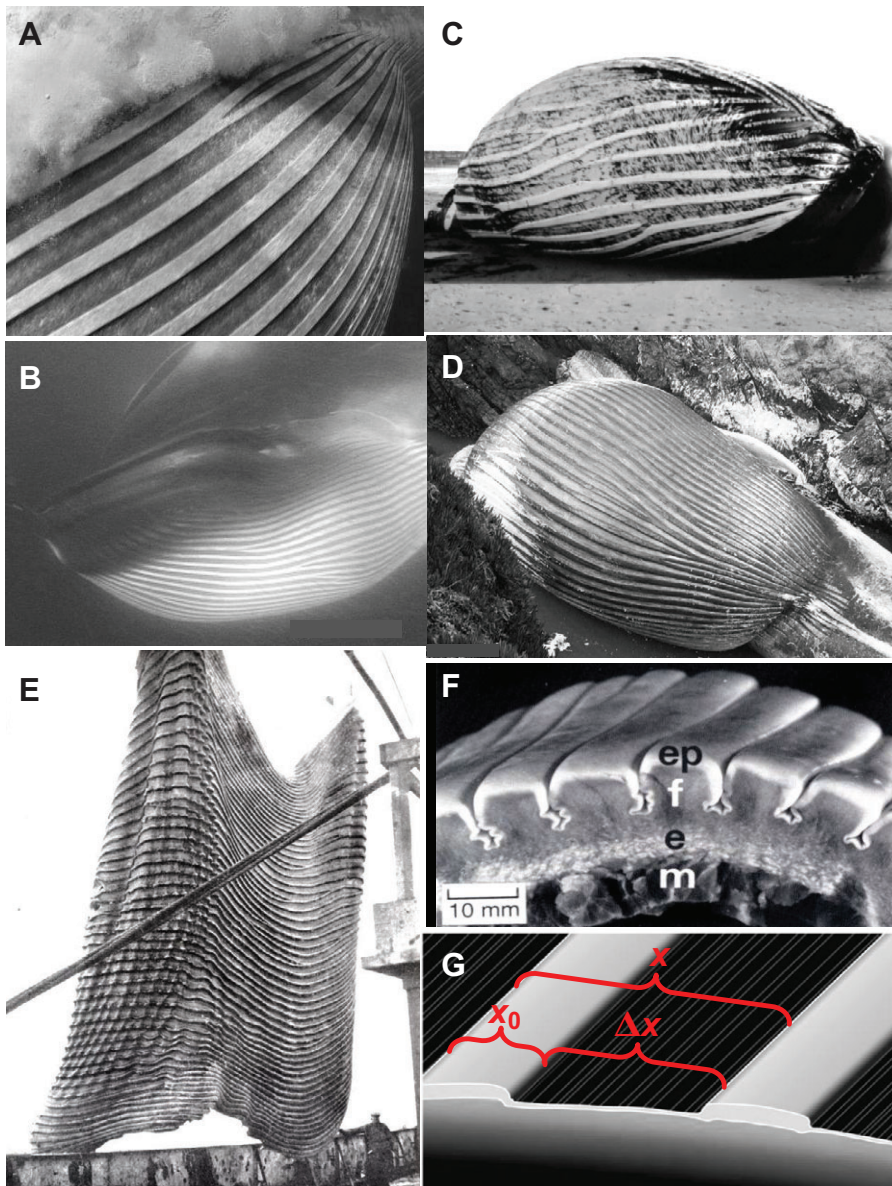


Fig. 3. Examples of images used to measure maximal transverse strain in the VGB. (A) Bryde's whale and (B) fin whale at full engulfment. (C) Humpback whale and (D) blue whale, bloated post-mortem. Photo credits: (A) Doug Perrine/SeaPics.com; (B) Claudio Valerio; (C) Arlene Erven; and (D) Ron LeValley. (E) Hanging blue whale 'blubber blanket' on an Antarctic whaling vessel (from Villiers, 1925). (F) A transverse section of the VGB from a small minke whale showing epidermal (ep), fatty and fibrous (f), elastin (e) and subdermal muscle (m) layers. Reprinted from de Bakker et al. (de Bakker et al., 1997) with permission. (G) A drawing of expanded VGB showing how deformation occurs in the grooves between the stiff ridges. The stretched length ( $x$ ) is equal to the initial length ( $x_0$ ) plus the increase in length ( $\Delta x$ ). Transverse strain is calculated as  $\epsilon_{Tmeas} = \Delta x/x_0$ . Reprinted from Goldbogen (Goldbogen, 2010) with permission.

walled cylinder, and using the stress–strain relationship for the VGB, they calculated that a lunge speed of  $3 \text{ m s}^{-1}$  would be sufficient in this 'passive engulfment' model. A recent tag study on lunge-feeding fin whales revealed a peak speed of  $3 \text{ m s}^{-1}$  before mouth opening (Goldbogen et al., 2006), seeming to corroborate the passive engulfment model (Goldbogen et al., 2007). In this model, for any lunge comprising engulfment through a complete mouth opening and closing cycle, the engulfed water mass must also be rapidly set into forward motion, a function attributed in the passive model to elastic loading and unloading of the VGB (Orton and Brodie, 1987; Simon et al., 2012). However, recent unsteady hydro-mechanical models of this process suggest that the highly compliant nature of the VGB would require all the water collected in the fully expanded ventral cavity (posterior to the temporal mandibular joint; Fig. 1) to be rapidly accelerated to the same speed as the whale once the elastic limit of the VGB was reached, thus requiring very large VGB extensions to provide the high forces needed (Potvin et al., 2009; Potvin et al., 2012). Furthermore, it was determined that engulfment by passive VGB inflation would result in drag forces too low to

decelerate the whale as quickly as was observed in direct field measurements (Goldbogen et al., 2006). Thus, an alternative mechanism of 'active engulfment' was proposed, in which the VGB muscles actively resist and control the rate of VGB expansion, accelerating the water mass more gradually, reducing peak drag forces and providing decelerations that matched the measured range (Potvin et al., 2009). In addition, evidence of mechanoreceptors in the VGB blubber and muscle layers (de Bakker et al., 1997) and in the mandibular symphysis (Pyenson et al., 2012) suggests that rorquals can sense the stretch of the tissue and the gape of the jaws, providing the sensory input needed to control active engulfment.

Images of dead rorquals often show a distended and relaxed VGB, which may droop under its own weight when on land [fig. 2 in Goldbogen (Goldbogen, 2010)], suggesting that in life the muscles must be important in preventing the VGB from sagging. Orton and Brodie (Orton and Brodie, 1987) proposed that VGB muscles must perform a postural role, arguing that a rorqual swimming with a closed mouth would experience a Bernoulli effect from water passing around the body, tending to pull the VGB outward.

Furthermore, they suggested the lack of muscle tone in a fresh dead animal was responsible for their observation of '2m thick rolls of bulging tissue in the ventral groove region in dead whales being towed to shore ...' by a whaling ship (Orton and Brodie, 1987). Finally, the VGB muscles are also likely involved in the filtration phase of lunge feeding by shortening to assist the elastic recoil of the VGB and forcing water through the baleen plates. Although these lines of evidence suggest that the VGB muscles serve a variety of critical functions during lunge-feeding, their anatomy remains poorly understood.

In this study we pose the hypothesis that VGB expansion during engulfment is controlled by eccentric muscle contraction that then sets the limit to the maximum volume engulfed. In practical terms, this idea is logistically impossible to test directly, so we used two indirect approaches. First, we used a geometric model of body dimensions to predict the maximum distension of the ventral cavity in four representative rorqual species, and then estimated the resulting transverse and longitudinal VGB strains. Second, we measured VGB strain *in vivo* from the relative separation of adjacent ridges seen in photos of various lunge-feeding rorquals. Calculated and measured VGB strains were in good agreement, and well below the limit imposed by collagen in passive stretch and predicted by the passive engulfment model. We also note that, in dead rorquals, VGB expansion is substantially higher in the absence of active muscle.

In addition, we address a potential functional problem for the VGB muscles. During engulfment, the underlying muscle layers must expand with the VGB to strains that could be untenable for skeletal muscle cells. It is unknown how the muscle layers are able to accommodate the large deformations that appear to be imposed by routine engulfment. Here we explore the structural organization of the VGB muscle layers and show how an unusual pairing with elastin fibres creates a geometry that allows large tissue expansion without excessive stretch of individual muscle cells. This analysis also suggests that the maximum extension of the VGB allowed by the connective tissue matrix is far greater than maximal strains likely allowed by muscle cells. This implication further questions the validity of passive inflation as a potential mechanism for engulfment.

## MATERIALS AND METHODS

### Calculation of VGB strains from ventral cavity volume models

We surveyed images and videos of various rorqual species lunge feeding collected from list-server requests and our own specific searches online. From these, a geometrical model was developed to represent the shape of the ventral pouch at full engulfment, in order to calculate the maximal engulfed volume (see Goldbogen et al., 2010). This model approximates the expanded pouch as two quarter ellipsoid volumes; one is anterior to the temporomandibular joint (TMJ; the pivot point between the mandible and skull), and the other is posterior to the TMJ (Fig. 1). This configuration allows us to calculate the maximal VGB strain in the longitudinal and transverse directions along the perimeter of the ellipses defined by the axes, as in Fig. 1B. We define strain ( $\epsilon$ ) as the change in a dimension relative to the original dimension (e.g.  $\epsilon = \Delta x/x_0$ ), so that a strain of 1.0 means a doubling of the initial dimension. For the longitudinal strain  $\epsilon_L$  we equate the stretched length of the VGB as the perimeter of the two quarter ellipsoids along the body long axis, as seen in lateral view (dashed lines in Fig. 1A), while its unstretched length is simply equal to  $L_{VGB}$ . For the transverse strain  $\epsilon_T$  we approximated the stretched length as the perimeter of half the ellipse in the transverse plane (solid white line in Fig. 1B, blue line in Fig. 4), and the unstretched length as the half of the perimeter of a circle

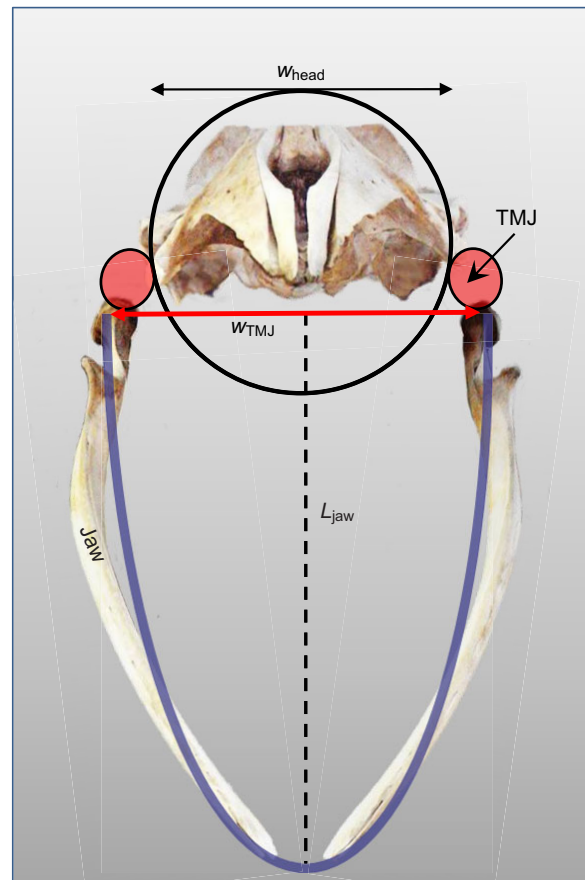


Fig. 4. Frontal view of the skull and mandibles of a minke whale with mandibles (jaws) open to a gape of  $\sim 50$  deg (specimen FOS2023 at the UBC Aquatic Ecosystems Research Laboratory). Mandibles articulate with the skull *via* fibro-elastic temporomandibular joint (TMJ) pads, which facilitate lateral displacement of the mandibular condyles during mouth opening. Blue line shows the half-ellipse used to approximate the mouth opening with the major axis equal to  $L_{\text{jaw}}$  (lateral projected length of the jaw) and the minor axis equal to  $w_{\text{TMJ}}$  (distance between the condyles when jaws open). This was determined to be 20% wider than  $w_{\text{head}}$  by preliminary post-mortem experiments. With the mouth closed, the head is modelled as a cylinder with diameter  $w_{\text{head}}$ .

with diameter equal to the width of the head ( $w_{\text{head}}$ ; Fig. 4) (Bose and Lien, 1989). For the minor ellipse axis in the transverse plane we used the width across the mandibular condyles ( $w_{\text{TMJ}}$ ; Fig. 4), which increases with gape to  $\sim 1.2$  times the width of the head, based on measurements we made on a fresh fin whale carcass (R.E.S., N.D.P. and J.A.G., unpublished). Ellipse perimeters were calculated using the Ramanujan approximation (Ramanujan, 1913-1914):

$$P_{\text{Ram}} \approx \pi \left[ 3(a+b) - \sqrt{(a+3b)(3a+b)} \right] k, \quad (1)$$

where  $a$  and  $b$  are the major and minor radii, respectively, of the ellipse, and  $k$  is set to 0.5 or 0.25 for calculating the perimeter of a half or quarter ellipse, respectively. Calculations of VGB strains were made for the average body size (i.e. total length in metres) of each of four species that span the range of average body size among the rorquals (Goldbogen et al., 2010; Potvin et al., 2012): minke (*B. acutorostrata* Lacepede 1804), 7.75 m; humpback (*Megaptera novaeangliae* Borowski 1781), 14.4 m; fin [*B. physalus* (Linnaeus 1758)], 20 m; and blue [*B. musculus* (Linnaeus 1758)], 25 m.

Table 1. Dimensions for average size whales, and calculated VGB strains ( $\epsilon_T$  and  $\epsilon_L$ ), based on the geometrical model of ellipse perimeters (Figs 1, 4)

	Minke ( <i>B. acutorostrata</i> )	Humpback ( <i>M. novaeangliae</i> )	Fin ( <i>B. physalus</i> )	Blue ( <i>B. musculus</i> )
$L_{\text{body}}$	7.75	14.4	20	25
$L_{\text{VGB}}$	3.54	8.64	11.3	14.7
$L_{\text{jaw}}$	1.44	3.28	3.95	5.0
$W_{\text{head}}$	0.86	2.41	2.18	2.96
$W_{\text{TMJ}}$	1.03	2.90	2.62	3.55
Transverse				
Stretched VGB	3.38	8.1	8.8	11.7
Rest length	1.41	3.8	3.42	4.65
$\epsilon_T$	1.40	1.12	1.57	1.52
Longitudinal				
Ant-TMJ $\frac{1}{4}$ perim.	2.32	5.25	6.40	8.05
Post-TMJ $\frac{1}{4}$ perim.	2.71	6.88	9.20	12.01
Stretched VGB	5.03	12.13	15.60	20.06
Rest length (=LVGB)	3.54	8.64	11.3	14.7
$\epsilon_L$	0.42	0.40	0.38	0.36

All dimensions are in metres; strain values have no units.  $L_{\text{body}}$ ,  $L_{\text{VGB}}$ ,  $L_{\text{jaw}}$  and  $W_{\text{head}}$  are from summaries in Goldbogen et al. (Goldbogen et al., 2010) and Potvin et al. (Potvin et al., 2012);  $W_{\text{TMJ}}$  is approximated as  $1.2 \times W_{\text{head}}$ .

### Measurement of VGB strain from images of whales

For comparison of predicted VGB strains with *in vivo* values, we searched for published images of various rorquals performing sub-surface lunge feeding where we judged the ventral cavity to be maximally distended. These included minke, Bryde's (*B. edeni* Anderson 1879/*B. brydei* Olson 1913), sei (*B. borealis* Lesson 1828), fin and blue whales. No suitable images were found for humpback whales. From 17 images (four each of blues, fins and Bryde's; three of minkes; two of seis) we determined VGB strain in the transverse direction ( $\epsilon_{T\text{meas}}$ ) by measuring separation of the ridges, as shown in Fig. 2. We typically measured across three to six ridges and sampled four to five areas in order to find the greatest value in each image. This technique relies on the fact that the lateral stretch of the VGB occurs between the stiff ridges, as was shown by direct mechanical tests on VGB samples (Orton and Brodie, 1987). Unfortunately, there was no reliable way to determine longitudinal strain from these images.

For comparison with engulfment, we also analysed 11 images of dead whales (four of humpbacks, three each of fins and blues, one

minke) in which the ventral cavity was bloated due to internal decomposition, presumably expanding the VGB to its passive elastic limit in the absence of muscle activity. With this method we obtained data for blue, fin and humpback whales. In one additional case we were able to measure maximal VGB strain from an image of a complete sheet of ventral 'blubber blanket' freshly flensed from a blue whale and hoisted up by its lateral edge so that the tissue mass caused strain in the transverse direction (Fig. 3E), most notably in the top-most portion.

### VGB muscle anatomy and histology

Gross dissections were made on five adult fin whale carcasses (total length range: 18–21 m) at a commercial whaling station at Hvalfjörður, Iceland, in July 2010. We measured the thickness of the two major layers of muscle that underlie the VGB – the OS and the LS (see Fig. 2) – documenting the thickness of these layers as a function of position along the body.

Samples of the VGB muscles from adult fin whales and from two adult minke whales (obtained from Hrefnuveiðimenn ehf, Hafnarfjörður, Iceland) were fixed in 10% buffered formalin for histological processing. Standard wax sections were cut at  $7\mu\text{m}$ , and stained with Verhoeff's van Gieson stain to distinguish elastin, collagen and muscle cells. Some muscle pieces were frozen on dry ice for histochemistry to distinguish muscle fibre types, using an acid (pH 4.3) and alkaline (pH 9.4) pre-incubation method to stain myosin ATPase (Brooke and Kaiser, 1970). All sections were viewed and photographed with a Zeiss Imager.A1 microscope

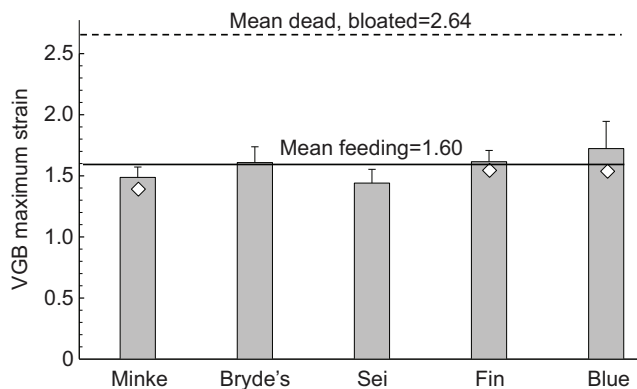


Fig. 5. Maximal transverse VGB strain ( $\epsilon_{T\text{meas}}$ ) measured from images of five balaenopterid species during lunge feeding (mean + s.d.;  $N=4$  for blue, fin and Bryde's, 3 for minke, 2 for sei). The overall mean maximal  $\epsilon_{T\text{meas}}$  was  $1.60 \pm 0.16$  during feeding and  $2.64 \pm 0.22$  in dead, bloated whales (see Table 2). Values of  $\epsilon_T$  calculated from the geometric model for minke, fin and blue whales (from Table 1) are also shown ( $\diamond$ ).

Table 2. Maximal transverse VGB strain ( $\epsilon_{T\text{meas}}$ ) calculated from images, as in Fig. 3, for full engulfment and for dead, bloated carcasses

Species	Fully engulfed	Dead, bloated
Minke ( <i>B. acutorostrata</i> )	1.49±0.09	
Bryde's ( <i>B. edeni/brydei</i> )	1.61±0.13	
Humpback ( <i>M. novaeangliae</i> )	n.a.	2.52±0.22
Sei ( <i>B. borealis</i> )	1.44±0.11	
Fin ( <i>B. physalus</i> )	1.62±0.10	2.59±0.15
Blue ( <i>B. musculus</i> )	1.72±0.22	2.81±0.19

Data are means ± s.d. of  $N=2-4$  per species. n.a., not available.

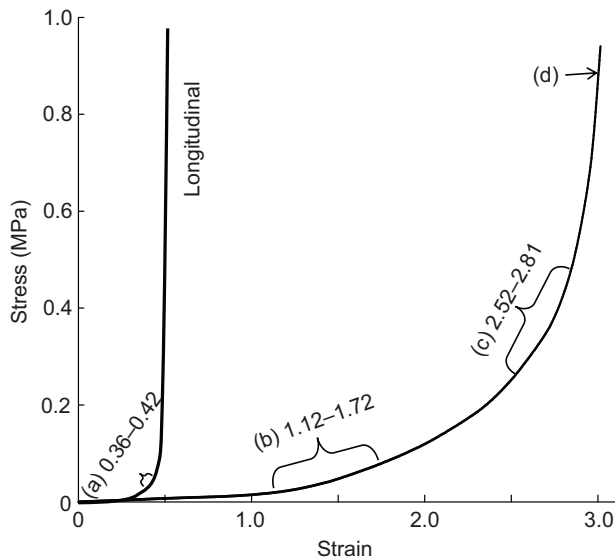


Fig. 6. The passive elastic properties of excised fin whale VGB, showing stress versus strain for the longitudinal and transverse directions (redrawn from Orton and Brodie, 1987). For comparison, the range of maximal values we calculated from the elliptical model of VGB expansion are shown: (a)  $\epsilon_L$  from Table 1; (b)  $\epsilon_T$  and  $\epsilon_{Tmeas}$  for full engulfment from Tables 1, 2; (c) maximal  $\epsilon_{Tmeas}$  for post-mortem bloated carcasses (Table 2); and (d) blue whale 'blubber blanket' from Fig. 2E.

(Jena, Germany) fitted with a Hitachi HV22 digital camera (Tokyo, Japan).

**RESULTS**

**Engulfment VGB strains calculated from geometry**

Based on the geometric analysis outlined above we calculated maximal transverse and longitudinal perimeters, and hence corresponding strains, of the VGB at full engulfment for representatives of four whale species, as shown in Table 1. Values of maximal  $\epsilon_L$  ranged from 0.36 to 0.42. For the transverse direction maximal,  $\epsilon_T$  was larger in *Balaenoptera* spp. (1.40–1.57) than in the humpback whale (1.12), which has a proportionately wider head (Table 1).

**Measured VGB strain during engulfment and in post-mortem bloated whales**

Examples of the types of images used to determine the transverse VGB strain ( $\epsilon_{Tmeas}$ ) in live whales at full engulfment and in post-mortem bloated whales are shown in Fig. 3. This comparison was made to determine the extent to which active muscle may limit VGB expansion during engulfment. Maximal engulfment  $\epsilon_{Tmeas}$  from images of live whales ranged from 1.49 to 1.72, with an overall mean of  $1.60 \pm 0.16$  (Fig. 5, Table 2). Images of extremely bloated dead specimens yielded estimates of maximal VGB expansion greatly exceeding those for engulfment, with  $\epsilon_{Tmeas}$  averaging  $2.64 \pm 0.22$  (Fig. 5, Table 2). In the gravity-loaded VGB 'blanket' from a blue whale, the separation of ventral grooves reached a strain of  $\sim 3.0$  (i.e. four times the unstretched length), corresponding closely to the elastic limit measured in previous tensile tests of fin whale VGB (Orton and Brodie, 1987) (see Fig. 6).

**Structure of muscle layers within the VGB**

Beneath the VGB and well attached to it are two major muscle groups that together can be more than 30 cm in combined thickness in 18–21 m fin whales, where blubber thickness is 9–15 cm (Fig. 7). Most superficial is the OS, which runs from the anterior-most part of the VGB, behind the mandibular symphysis, to its posterior margin near the umbilicus, attaining a maximal thickness of 10–14 cm (Fig. 7). This contains bundles of muscle cells that occur in a series of layers lying alternately at +45 and -45 deg to the body long axis, interspersed with large amounts of lipid and collagenous connective tissue (Figs 2, 7). The OS is likely composed of the mylohyoideus and/or panniculus muscle groups (Schulte, 1916; Pivorunas, 1977; Lambertsen, 1983; Orton and Brodie, 1987). Adjacent and deep to the OS is an LS that runs posteriorly from the mandibular symphysis to approximately the longitudinal mid-point of the VGB (Pivorunas, 1977) (see also Fig. 7), with maximal thickness of 11–24 cm. The LS is composed of muscle bundles of 1–2 cm diameter that are very loosely connected to each other (see Figs 2, 7), and can easily be separated laterally as well as stretched. Bundles in the OS are of similar size but more tightly packed; the large amount of intervening fat and connective tissue allows for relatively easy deformation along and transverse to the body long axis. These observations indicate on a gross level how the muscles are predisposed to deform readily during engulfment.

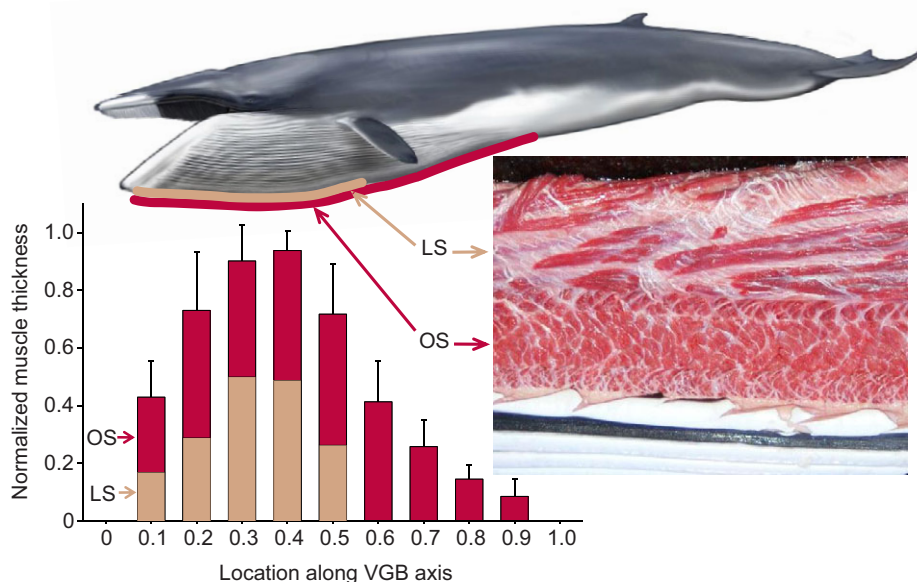


Fig. 7. Distribution of VGB muscle strata. The oblique stratum (OS) extends from approximately 0.1 to 0.9 of the full VGB length. The longitudinal stratum (LS) lies deep to the OS but extends posteriorly to only approximately 0.5 of the VGB length. The histogram shows the relative proportions of OS and LS (means + s.d.;  $N=5$ ), normalized to the maximum thickness of the muscle layers (at 0.4 of VGB length). The photo on the right shows a longitudinal section through the VGB in an adult fin whale, post-mortem with the blubber layer at the bottom. Artwork courtesy of Carl Buell.

Histological examination shows that the cells within both VGB muscle strata are similar in size, with diameters ranging from approximately 50 to 90  $\mu\text{m}$  (Figs 8–10). The microstructure affords some insights into the unusual nature of the VGB muscles. Most notable is the preponderance of predominantly straight elastin fibres within the connective tissue space between the muscle cells of the OS (Sokolov, 1960; Orton and Brodie, 1987) (Fig. 8, Fig. 10A,B), particularly in the fin whale, where these fibres are very dense and up to 8  $\mu\text{m}$  in diameter (Fig. 8). In addition, the OS muscle cells in the fin whale are highly crimped in the unloaded state while the elastin fibres are straight, suggesting that recoil of the elastin has caused longitudinal compression of the muscle (Fig. 8B,C). Note also that the crimping is fairly regular along the muscle length as if the cells have areas predisposed to accommodate the longitudinal compression. This is also evident in the minke OS (Fig. 10A,B), but to a lesser extent. In contrast, the LS muscle contains very little elastin and has a lower incidence of crimping in both species. To quantify this feature we calculated the ‘waviness index’ (Table 3) as the traced contour length of a muscle cell segment divided by its straight path length in the image (Lillie and Gosline, 2006). For example, this metric shows that if the longitudinal crimping caused by the elastin was removed, muscle fibre lengths would increase

by approximately 35% in the fin OS but only by 7% in the minke LS.

Differentiation of Type I slow-twitch and Type II fast-twitch muscle (or oxidative fatigue resistant and glycolytic burst muscle, respectively) was successful for OS and LS from minke whales only (see Fig. 11), thus an inter-specific comparison is not possible here. We determined the proportion of dark stained fibres from counts of >150 fibres in each section (two sections per slide, two slides per muscle type per animal) and observed that both muscle strata had mixed fibre populations with slow-twitch fibres comprising ~63% of the OS and 42% in the LS. This contrasts with a similar measurement in the fin whale (Orton and Brodie, 1987), where oxidative fibres were reported to comprise ~55% of the OS and up to 95% of the LS. These data may not be directly comparable, as we do not know whether the fibre type distribution is dependent on location within the muscle strata. Moreover, a recent study (Potvin et al., 2012) suggests that the oxidative capability of the VGB muscles may be strongly dependent on species and size, as the metabolic power during engulfment comes closer to the aerobic limit at large body size. Therefore, one might expect greater proportions of glycolytic fibres in VGB muscles of the larger fin and blue whales than for minke whales, but this awaits further study.

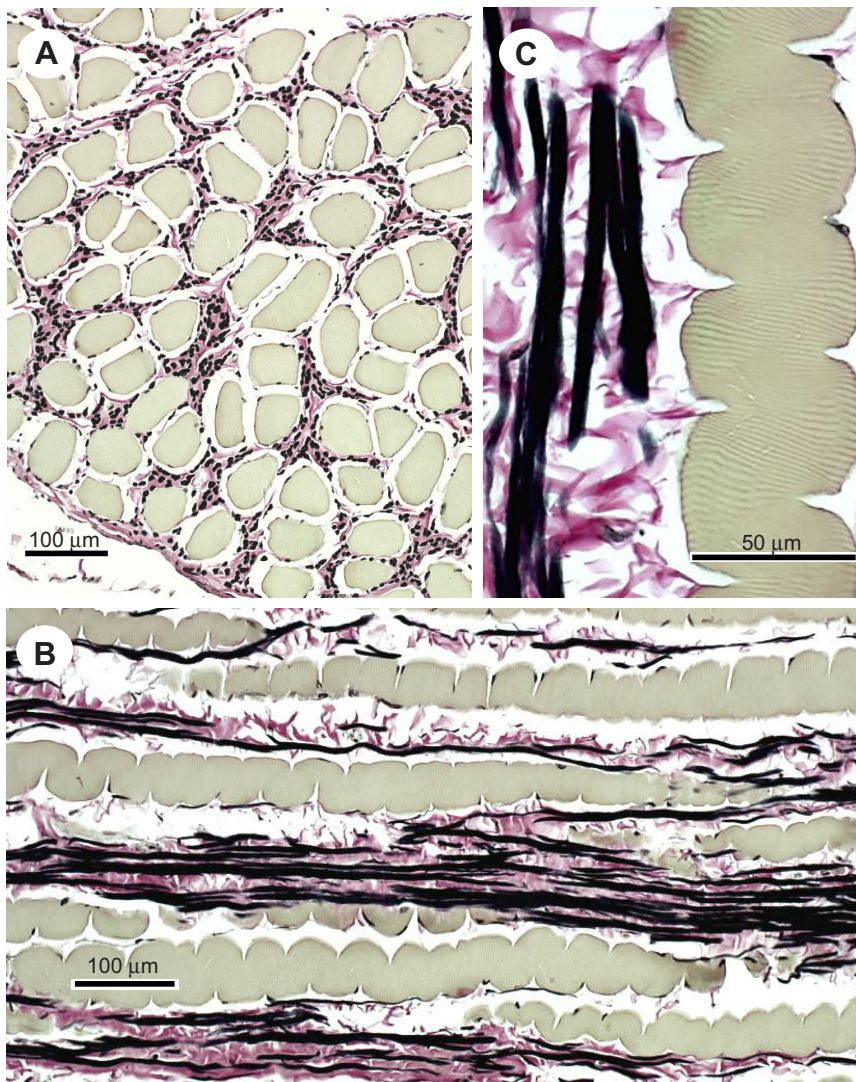


Fig. 8. Histological transverse (A) and longitudinal (B,C) sections of oblique muscle stratum from a fin whale stained with Verhoeff's van Gieson to show cells (yellow-brown), elastin fibres (black) and collagen (purple). These muscle cells are embedding in a dense connective tissue matrix and have a crimped appearance at rest.

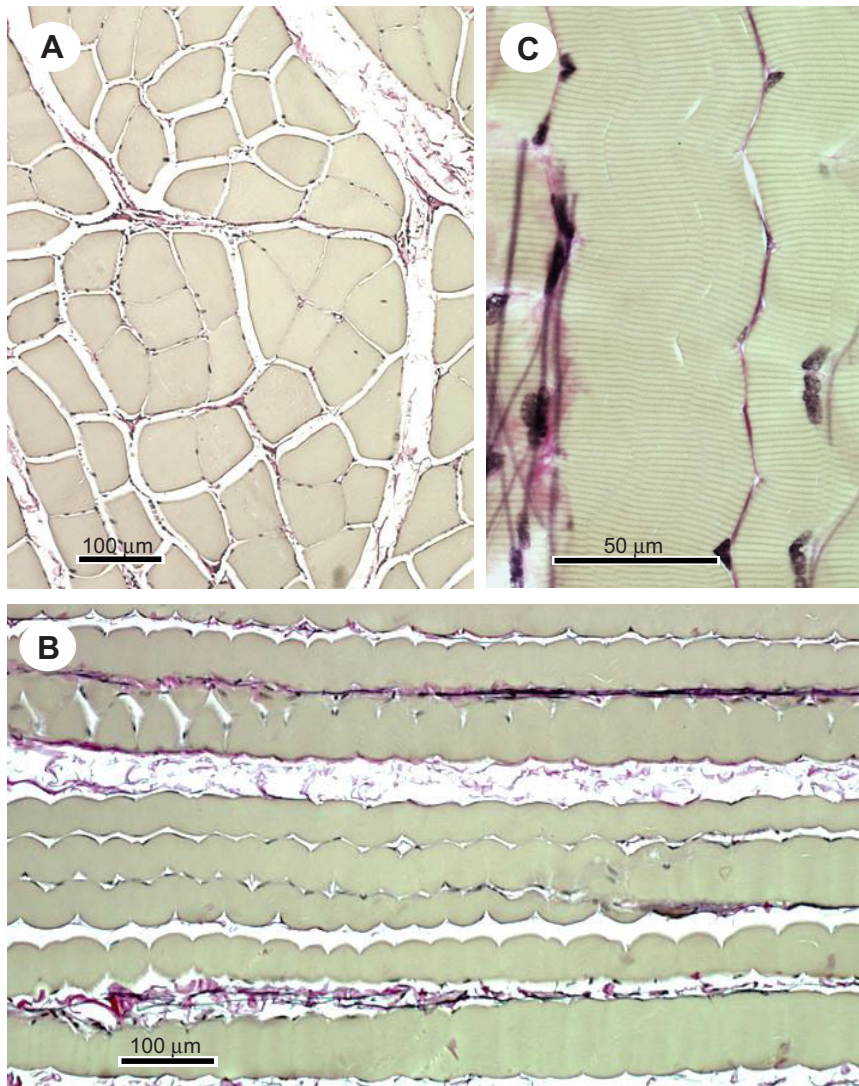


Fig. 9. Histological transverse (A) and longitudinal (B,C) sections of longitudinal muscle stratum from a fin whale stained with Verhoeff's van Gieson to show cells (yellow-brown), elastin fibres (black) and collagen (purple). Compared with the OS, these muscle cells are less crimped and have much less elastin and collagen matrix.

## DISCUSSION

### VGB strains during engulfment

The evidence presented here lends support to our hypothesis that engulfment volume is not set by the passive elastic properties of the VGB. Rather, routine full engulfment requires VGB deformation that is much lower than the elastic limit of the tissue, and therefore the engulfment dynamics must be controlled by the action of VGB muscles. The VGB is an anisotropic elastic structure that expands much more in the transverse direction than longitudinally, a behaviour that is directly linked to the influence of the longitudinal grooves (Orton and Brodie, 1987). Our estimates of  $\epsilon_L$  from the geometric model ( $\sim 0.36$ – $0.42$ ) are less than the maximum  $\epsilon_L$  of VGB obtained previously in longitudinal tests ( $\sim 0.5$ ; see Fig. 6). More importantly, our estimates of  $\epsilon_T$  for balaenopterids (Table 1) are quite close to those measured from images of expanded pleats during lunge feeding (Table 2), supporting the ellipsoid model as a good approximation of the engulfment geometry. This level of transverse strain is high for a biological tissue, but much less than the maximum we found in images of post-mortem bloated whales ( $\sim 2.64$ ). Interestingly, the maximum transverse strain recorded in tensile tests of excised slabs of VGB approached 3.0 (Fig. 6), also coinciding with the maximum  $\epsilon_{T\text{meas}}$  for the hanging 'blubber blanket' (Fig. 3E), which we take to be fully extended. This suggests that the post-

mortem bloated condition may cause nearly complete expansion of the VGB, close to or at its elastic limit (e.g. Fig. 6), but routine lunge feeding involves only sub-maximal strains, most likely because the underlying muscles actively control the VGB stretch during engulfment. Such a scenario is consistent with predictions from models of engulfment dynamics of fin whales (Potvin et al., 2009; Potvin et al., 2010; Potvin et al., 2012). In these simulations, different rates of ventral cavity filling, based on passive or differing levels of active control, resulted in corresponding body decelerations that were compared with the deceleration of lunge-feeding whales measured using digital tags. Only simulations with active control of VGB expansion agreed with the measured velocity data, while the case of passive inflation led to over-filling and reflux of the engulfed volume during mouth closure (Potvin et al., 2009; Potvin et al., 2010; Potvin et al., 2012). Furthermore, if routine full engulfment did expand VGB to its elastic limit ( $\epsilon_T$  of 2.5–3.0), we estimate this would double the volume of water engulfed, leading to a doubling of drag forces and unrealistic power requirements to perform lunges (Goldbogen et al., 2012; Potvin et al., 2012).

### How can the muscles accommodate large VGB strains?

Orton and Brodie (Orton and Brodie, 1987) proposed two mechanisms to explain how the VGB muscle layers might undergo

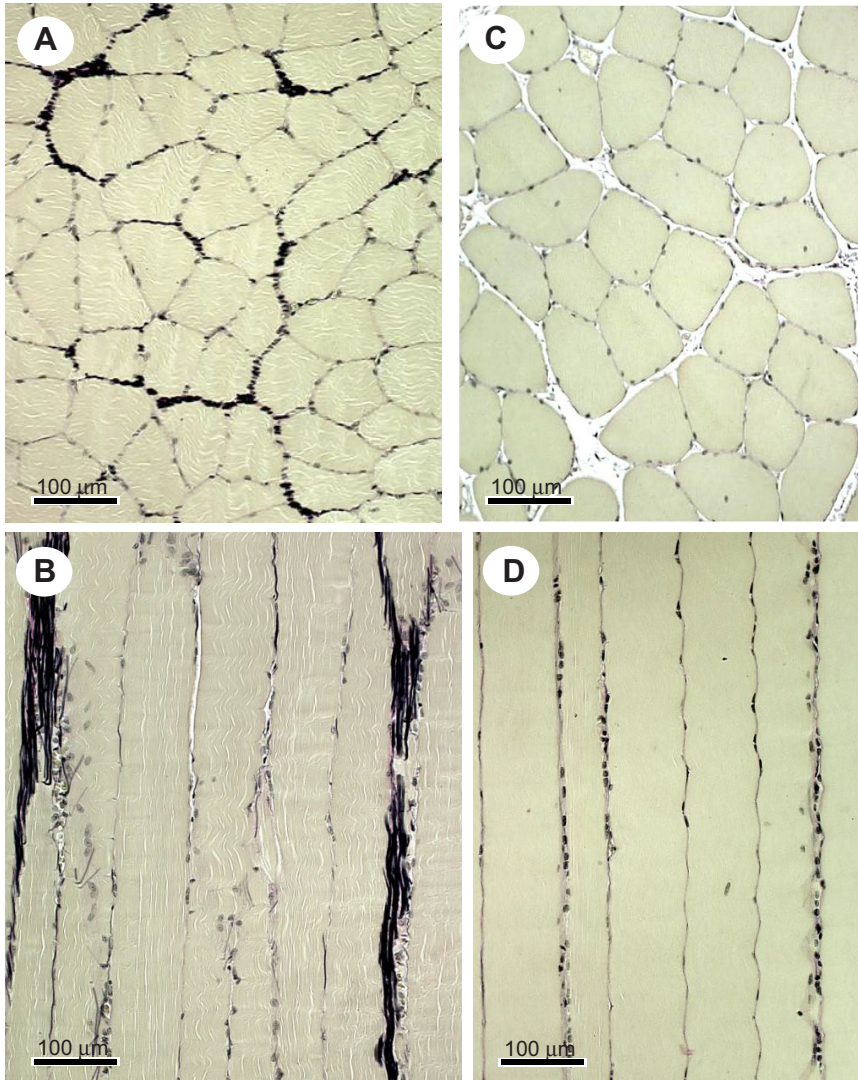


Fig. 10. Histological transverse (A,C) and longitudinal (B,D) sections of OS (A,B) and LS (C,D) muscle from a minke whale stained with Verhoeff's van Gieson to show cells (yellow-brown), elastin fibres (black) and collagen (purple). Elastin fibres are dense in OS but scarce in LS. Longitudinal crimping is less prominent than in fin whale sections (see Figs 8, 9).

extreme deformations. Their tensile tests on large bundles of fin whale OS and LS demonstrated a recoverable extensibility that was comparable to that of the VGB, i.e. the LS and OS bundles could be stretched up to strains of  $\approx 2.4$  (but this would yield sarcomere lengths  $\gg 6\mu\text{m}$ ). The simplest possibility they suggested was that the VGB muscle cells are unusually capable of sustaining extreme stretch, but they provided no structural evidence to support this contention, nor has any emerged from any vertebrate skeletal muscle to date. As the muscles in those tests were dead, the recoil was undoubtedly due to the supporting elastic connective tissue matrix in the strata (see Figs 8–10). Alternatively, these same authors proposed that the VGB muscle cells may be much shorter than the lengths of the large bundles tested and linked together in series by the elastin network so that much of the macroscopic strain is accounted for by stretching of elastin, not the muscle cells. This morphology is not supported by the structural evidence in our study, which indicates a parallel arrangement of muscle and elastin.

Our new results provide the basis for formulating an analysis of how the VGB muscles function during lunge feeding. Using a simple geometric representation of the VGB components for a fin whale we can calculate strain in the muscle strata and elastin fibres as the ventral cavity expands. Fig. 12 shows a representation of a

$1\times 1$  unit section of VGB, from the region of maximal expansion during engulfment (i.e. along the ventral midline at about the level of the TMJ; see Fig. 1) with LS muscle oriented along the body axis, OS muscle initially at 45 deg and elastin fibres parallel to the OS. Thus, the initial path lengths of LS and OS will be 1.0 and 1.41, respectively. We assume final dimensions at full engulfment to yield  $\epsilon_T$  of 1.60 and  $\epsilon_L$  of 0.38 (Tables 1, 2). It is immediately apparent that no muscles are subjected to the full transverse VGB strain of 1.60, because none lie along the transverse axis. If extension of muscle cells was the same as for the VGB (i.e. if there was no initial muscle crimping) then, according to Fig. 12, the LS muscle would lengthen by approximately 38% (i.e. from 1.0 to 1.38;  $\epsilon=0.38$ ); OS muscle and elastin fibres would double in length

Table 3. Waviness index for OS and LS calculated from longitudinal sections of muscle fibres, as the contour length/straight path length

Species	OS	LS
Minke ( <i>B. acutorostrata</i> )	1.15 $\pm$ 0.03	1.07 $\pm$ 0.03
Fin ( <i>B. physalus</i> )	1.35 $\pm$ 0.09	1.13 $\pm$ 0.04

Measurements are means  $\pm$  s.d. from six muscle fibres from each type and species.

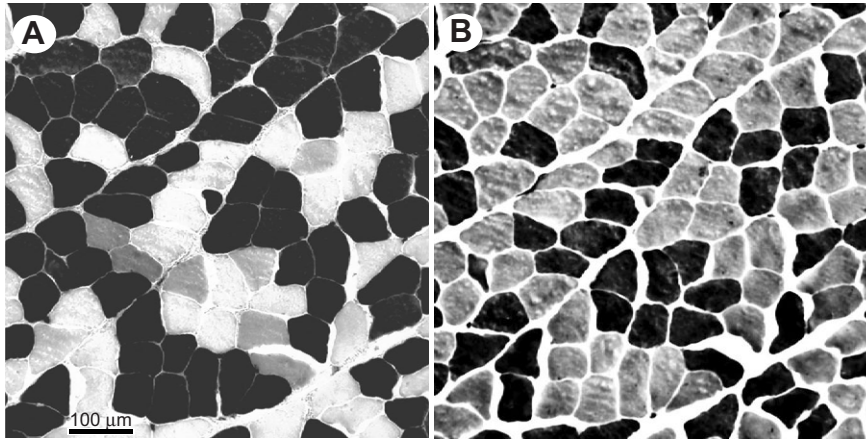


Fig. 11. Serial sections of OS muscle from a minke whale stained with Myosin ATPase after (A) pH 4.3 pre-incubation (Type I fibres stained dark) and (B) pH 9.4 pre-incubation (Type II fibres stained dark).

(i.e. from 1.41 to 2.94;  $\epsilon=1.09$ ). These predicted strains for LS and elastin fibres are reasonable (Aaron and Gosline, 1981), but not so for the OS, as a doubling would produce sarcomere lengths in the range of  $>4\mu\text{m}$  (based on resting sarcomere lengths of  $2.1\mu\text{m}$ ;

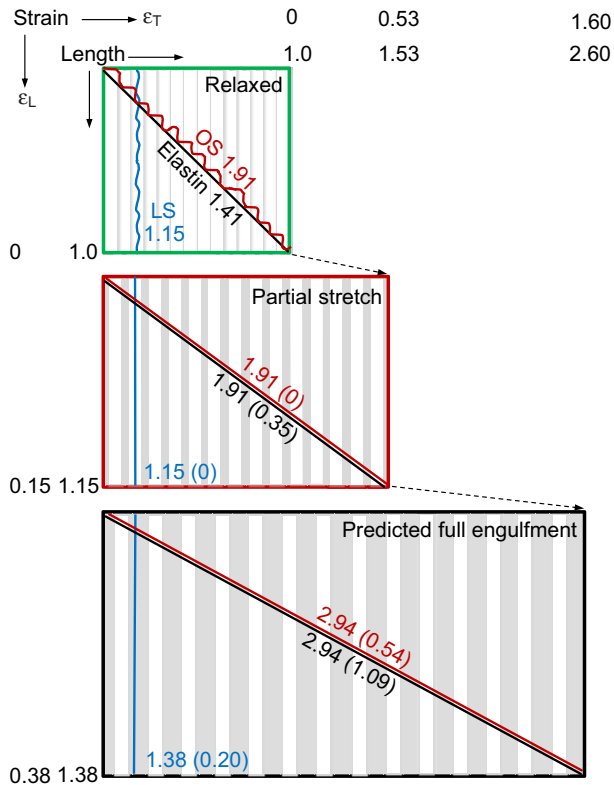


Fig. 12. Unit section of fin whale VGB represented as a square (green box, top); each side has a length of 1.0, so the diagonal length is 1.41. The longitudinal axis and LS (blue vertical crimped line) are in the vertical direction; OS (diagonal crimped red line) and elastin fibres (diagonal straight black line) are oriented at 45 deg. Straight elastin fibres are also present in the LS but in lower abundance, and are not shown here. Within the unit section in the relaxed state, diagonal elastin fibres will have a path length of 1.41, but OS muscle fibres will have a contour length of 1.91 because of the 1.35 waviness factor. Likewise, LS muscle fibres will have a contour length of 1.15. Partial expansion to  $\epsilon_L=0.15$  and  $\epsilon_T=0.53$  (red box, middle) will just uncrimp OS and LS muscle, but will stretch elastin to 1.91 ( $\approx+35\%$ ). Expansion of the VGB to predicted full engulfment (black box, bottom) will result in a transverse length of 2.60 ( $\epsilon_T=1.60$ , averaged from Tables 1, 2) and a longitudinal length of 1.38 ( $\epsilon_L=0.38$ , Table 1), imposing stretch on the muscle cells of +20 and +54% for LS and OS, respectively, and +109% on the elastin.

R.E.S., unpublished), where there would be no overlap between thick and thin filaments, no contractile force could be developed (ter Keurs et al., 1978; Herzog et al., 1992; Wang et al., 1993; Zuurbier et al., 1995) and myofibrillar damage would occur (Wang et al., 1993). However, the apparent compression of muscle cells by recoiling elastin fibres (Fig. 8, Table 3) relieves the problem for the OS because the initial VGB deformation would uncrimp but not stretch the cells. Our model shows that crimped OS muscle cells with a starting path length of 1.41 would reach a straightened length of 1.91 (per waviness index in Table 3) when VGB  $\epsilon_T=0.53$  and  $\epsilon_L=0.15$  (Fig. 12, red box). These cells would then stretch to 2.94 at full engulfment ( $\epsilon_T=1.60$ ,  $\epsilon_L=0.38$ ), a stretch of only 54%, which is quite feasible for skeletal muscle (ter Keurs et al., 1978; Herzog et al., 1992; Joumaa et al., 2008). Crimping in the LS is lower but would also reduce the actual strain of these muscle cells with VGB expansion. This results in LS muscle strain at full engulfment of only 20%. Our model, while a simplification of the actual anatomy, provides a plausible explanation of how the muscle cells accommodate the large extension of the VGB in lunge feeding, by a novel structural design.

The model in Fig. 12 also leads us to conclude that OS muscles could not sustain VGB transverse strains to the elastic limit, as seen in post-mortem samples (Fig. 6). If full engulfment actually reached such high transverse strains (i.e. 2.5–3.0), the OS fibres would be subjected to stretches of  $>100\%$ , or sarcomere lengths again approaching or exceeding  $4.0\mu\text{m}$ , where irreversible damage in myofibrils occurs (Wang et al., 1993). As expansion to near the elastic limit is necessary for a passive engulfment model, in order to provide the high forces required to accelerate large masses of engulfed water (Potvin et al., 2009; Potvin et al., 2012), our results do not support this scenario for routine full engulfment lunge feeding. In fact, we suggest that by having the elastic limit so far beyond the strains normally experienced in lunge feeding, passive stiffness remains low and muscle activation can be used to fully control the rate at which the VGB expands and fills. Given that the photographic data used in this study were from lunges performed nearly horizontally, a future goal will be to further assess the role of VGB muscles in other modes of lunge feeding, such as vertical lunges towards fish, as well as during the filtration process.

#### ACKNOWLEDGEMENTS

We would like to thank Kristján Loftsson, Dallí Halldórsson, Droplaug Ólafsdóttir and Gísli Víkingsson for help in Iceland, and Kristrún Ólafsdóttir for help with histochemistry. Stephen Raverty kindly aided our effort to recover tissue samples from the field. We also thank Danielle Duguid, Sandra Elizabeth, Arlene Erven, L. A. Holmes, Kaili Jackson, Kristen Jule, Teresa Mazza, Conor Ryan, Julius Schoen, and Claudio Valerio for supplying whale images for strain analysis.

## AUTHOR CONTRIBUTIONS

All authors contributed to developing concepts and collecting and analysing the data used here. After initial drafting by R.E.S., all other authors contributed to finalizing and revising the article.

## COMPETING INTERESTS

No competing interests declared.

## FUNDING

R.E.S. and A.W.V. acknowledge funding from the Natural Sciences and Engineering Research Council (NSERC) of Canada Discovery Grants Program. J.A.G. was supported by a Graduate Fellowship from the University of British Columbia and a Postdoctoral Fellowship from the Scripps Institution of Oceanography. N.D.P. was supported by an NSERC Postdoctoral Research Fellowship, the Smithsonian Institution, and its Remington Kellogg Fund.

## REFERENCES

- Aaron, B. B. and Gosline, J. M. (1981). Elastin as a random network elastomer. *Biopolymers* **20**, 1247-1260.
- Altringham, J. D., Wardle, C. S. and Smith, C. I. (1993). Myotomal muscle function at different locations in the body of a swimming fish. *J. Exp. Biol.* **182**, 191-206.
- Arnold, P. W., Birtles, R. A., Sobtzyck, S., Matthews, M. and Dunstan, A. (2005). Gulping behaviour in rorqual whales: underwater observations and functional interpretation. *Mem. Queensland Museum* **51**, 309-332.
- Biewener, A. A. (2003). *Animal Locomotion*. Oxford: Oxford University Press.
- Biewener, A. A., McGowan, C. P., Card, G. M. and Baudinette, R. V. (2004). Dynamics of leg muscle function in tammar wallabies (*M. eugenii*) during level versus incline hopping. *J. Exp. Biol.* **207**, 211-223.
- Bose, N. and Lien, J. (1989). Propulsion of a fin whale (*Balaenoptera physalus*): why the fin whale is a fast swimmer. *Proc. R. Soc. B* **237**, 175-200.
- Brooke, M. H. and Kaiser, K. K. (1970). Three 'myosin adenosine triphosphatase' systems: the nature of their pH lability and sulphydryl dependence. *J. Histochem. Cytochem.* **18**, 670-672.
- de Bakker, M. A. G., Kastelein, R. A. and Dubbeldam, J. L. (1997). Histology of the grooved ventral pouch of the minke whale, *Balaenoptera acutorostrata*, with special reference to the occurrence of lamellated corpuscles. *Can. J. Zool.* **75**, 563-567.
- Gillis, G. B. and Blob, R. W. (2001). How muscles accommodate movement in different physical environments: aquatic versus terrestrial locomotion in vertebrates. *Comp. Biochem. Physiol.* **131A**, 61-75.
- Goldbogen, J. A. (2010). The ultimate mouthful: lunge feeding in rorqual whales. *Am. Sci.* **98**, 124-131.
- Goldbogen, J. A., Calambokidis, J., Shadwick, R. E., Oleson, E. M., McDonald, M. A. and Hildebrand, J. A. (2006). Kinematics of foraging dives and lunge-feeding in fin whales. *J. Exp. Biol.* **209**, 1231-1244.
- Goldbogen, J. A., Pyenson, N. D. and Shadwick, R. E. (2007). Big gulps require high drag for fin whale lunge feeding. *Mar. Ecol. Prog. Ser.* **349**, 289-301.
- Goldbogen, J. A., Potvin, J. and Shadwick, R. E. (2010). Skull and buccal cavity allometry increase mass-specific engulfment capacity in fin whales. *Proc. R. Soc. B* **277**, 861-868.
- Goldbogen, J. A., Calambokidis, J., Croll, D., McKenna, M. F., Oleson, E., Potvin, J., Pyenson, N. D., Schorr, G., Shadwick, R. E. and Tershy, B. R. (2012). Scaling of lunge feeding performance in rorqual whales: mass-specific energy expenditure increases with body size and progressively limits diving capacity. *Funct. Ecol.* **26**, 216-226.
- Herzog, W., Kamal, S. and Clarke, H. D. (1992). Myofibril lengths of cat skeletal muscle: theoretical considerations and functional implications. *J. Biomech.* **25**, 945-948.
- Higham, T. E. and Biewener, A. A. (2008). Integration within and between muscles during terrestrial locomotion: effects of incline and speed. *J. Exp. Biol.* **211**, 2303-2316.
- Joumaa, V., Leonard, T. R. and Herzog, W. (2008). Residual force enhancement in myofibrils and sarcomeres. *Proc. R. Soc.* **275**, 1411-1419.
- Lambertsen, R. H. (1983). Internal mechanism of rorqual feeding. *J. Mammal.* **64**, 76-88.
- Lillie, M. A. and Gosline, J. M. (2006). Tensile residual strains on the elastic lamellae along the porcine thoracic aorta. *J. Vasc. Res.* **43**, 587-601.
- Orton, L. S. and Brodie, P. F. (1987). Engulfing mechanics of fin whales. *Can. J. Zool.* **65**, 2898-2907.
- Pivorunas, A. (1977). The fibrocartilage skeleton and related structures of the ventral pouch of balaenopterid whales. *J. Morphol.* **151**, 299-313.
- Potvin, J., Goldbogen, J. A. and Shadwick, R. E. (2009). Passive versus active engulfment: verdict from trajectory simulations of lunge-feeding fin whales *Balaenoptera physalus*. *J. R. Soc. Interface* **6**, 1005-1025.
- Potvin, J., Goldbogen, J. A. and Shadwick, R. E. (2010). Scaling of lunge feeding in rorqual whales: an integrated model of engulfment duration. *J. Theor. Biol.* **267**, 437-453.
- Potvin, J., Goldbogen, J. A. and Shadwick, R. E. (2012). Metabolic expenditures of lunge feeding rorquals across scale: implications for the evolution of filter feeding and the limits to maximum body size. *PLoS ONE* **7**, e44854.
- Pyenson, N. D., Goldbogen, J. A., Vogl, A. W., Szathmary, G., Drake, R. L. and Shadwick, R. E. (2012). Discovery of a sensory organ that coordinates lunge feeding in rorqual whales. *Nature* **485**, 498-501.
- Ramanujan, S. (1913-1914). Modular equations and approximations to  $\pi$ . *Quart. J. Pure Appl. Math.* **45**, 350-372.
- Schulte, H. W. (1916). The sei whale (*Balaenoptera borealis* Lesson). Anatomy of a foetus of *Balaenoptera borealis*. *Mem. Amer. Nat. Hist. New Series* **1**, 389-502.
- Simon, M., Johnson, M. and Madsen, P. T. (2012). Keeping momentum with a mouthful of water: behavior and kinematics of humpback whale lunge feeding. *J. Exp. Biol.* **215**, 3786-3798.
- Sokolov, W. (1960). Some similarities and dissimilarities in the structure of the skin among the suborders Odontoceti and Mysticoceti (Cetacea). *Nature* **185**, 745-747.
- Syme, D. A. (2006). Functional properties of skeletal muscle. In *Fish Physiology: Fish Biomechanics*, Vol. 23 (ed. R. E. Shadwick and G. V. Lauder; series ed. D. J. Randall and A. P. Farrell), pp. 179-240. San Diego, CA: Academic Press.
- ter Keurs, H. E., Iwazumi, T. and Pollack, G. H. (1978). The sarcomere length-tension relation in skeletal muscle. *J. Gen. Physiol.* **72**, 565-592.
- Villiers, A. J. (1925). *Whaling in the Frozen South*. Indianapolis, IN: McBride.
- Wang, K., McCarter, R., Wright, J., Beverly, J. and Ramirez-Mitchell, R. (1993). Viscoelasticity of the sarcomere matrix of skeletal muscles. The titin-myosin composite filament is a dual-stage molecular spring. *Biophys. J.* **64**, 1161-1177.
- Williamson, G. R. (1972). The true body shape of rorqual whales. *J. Zool.* **167**, 277-286.
- Zuurbier, C. J., Heslinga, J. W., Lee-de Groot, M. B. E. and Van der Laarse, W. J. (1995). Mean sarcomere length-force relationship of rat muscle fibre bundles. *J. Biomech.* **28**, 83-87.